Dynamic Average Modeling of Line-Commutated Converters for Power Systems Applications

IEEE Task Force on Dynamic Average Modeling
S. Chiniforoosh, J. Jatskevich (Chair), V. Dinavahi, R. Iravani, J. A. Martinez, A. Ramirez

Abstract— **Detailed switch-level models of high-pulse-count converters are relatively straightforward to implement using commonly available simulation packages used for digital time-domain simulations and studying of power systems transients. However, such models are computationally intensive due to switching, and could become the bottle-neck for system-level studies with large number of components and controllers. This paper describes approaches for developing dynamic average-value models, i.e., the analytical derivations and parametric modeling. The resulting approximate models do not represent switching but still capture the transient behavior of the original converter circuit. The paper presents the results for 3- and 6-phase rectifiers implemented in PSCAD/EMTDC and Matlab/Simulink and shows that dynamic average models can be very effective. The paper also shows that as the number of pulses/phases increases, so does the complexity of switching pattern that defines the operating modes.**

Index Terms-- **Average-value modeling, digital simulation, line-commutated converters, operational modes, rectifiers.**

I. Introduction

DETAILED models of high-pulse-count converters where switching of all semiconductor devices is represented can be readily carried out using available digital time-domain simulation packages [1]–[4]. The resulting models have been investigated in the literature quite extensively and are shown to be sufficiently accurate for many practical cases including 3-, 5-, and 6-phase configurations. However, due to the inherent repeated switching, these models are computationally intensive and could be the bottle-neck for the system-level studies that consider a large number of components and controllers. Moreover, detailed switching models are discontinuous and cannot be linearized and used effectively for the small-signal analysis. These challenges have lead to the development of the so-called average-value models (AVMs) in which the effect of fast switching is neglected (or averaged) within a prototypical switching interval. The AVMs described in this paper are based on averaging the ac currents and voltages in synchronously rotating *qd* coordinates, which implies that the switching harmonics are not represented on either ac side or the dc link side. In other words, the ac variables in *qd* coordinates and the dc link variables all appear constant in steady state.

The resulting models are computationally efficient and could run orders of magnitudes faster than the original switching models. Such AVMs can therefore be used for simulations of systems transients where the switching harmonics (i.e. the harmonics due to converter switching injected into the ac grid or the dc link) are neglected. Additionally, since AVMs are time-invariant, they can be linearized about any desired operating point for small-signal analysis, i.e., obtaining local transfer functions.

Construction of AVMs for line-commutated converters requires averaging of current/voltage waveforms over a prototypical switching interval, and may be carried out using several approaches. For example, in simplified cases where only certain operating modes are considered, such averaging may be done analytically [5]–[7]. However, as the number of pulses increases (which is the case when one considers 3-, 5-, and 6-phase configurations) the complexity of switching pattern and the number of possible operational modes increase as well. The possibility of multiple operating modes makes the analytical derivations quite challenging [8]–[11].

Average-value models may also be constructed using the parametric approach in which the final AVM is assumed to have a well-defined structure and the key model parameters are numerically extracted using the detailed simulations, thus avoiding the need for complicated analytical derivations. The resulting model is seamlessly functional in all operational modes. However, the detailed switch-level model of the system should be implemented first and run over a wide range of operating points to ensure that the parametric functions are extracted to cover the required range.

Regardless of the approach used to develop the AVM, once the AVM is constructed, it should be capable of predicting the average behavior of the detailed switching

S. Chiniforoosh and J. Jatskevich are with the Department of Electrical and Computer Engineering, The University of British Columbia, Vancouver, BC V6T1Z4 CANADA (e-mail: {sinach,jurij}@ece.ubc.ca).

Task Force on Dynamic Average Modeling is with the Working Group on Modeling and Analysis of System Transients Using Digital Programs, General Systems Subcommittee, T&D Committee, IEEE Power and Energy Society.

Task Force members: Abner Ramirez, Afshin Rezaei-Zare, Amirnaser Yazdani, Ani Gole, Houshang Karimi, Jean Mahseredjian, Juan Martinez, Juri Jatskevich (TF Chair), Karl Schoder, Luis Naredo, Michel Rioual, Reza Iravani, Sami A. Abdulsalam, Shaahin Filizadeh, Sina Chiniforoosh, Taku Noda, Venkata Dinavahi.

978-1-4244-4241-6/09/$25.00 ©2009 IEEE

converter circuit. The AVM is also computationally efficient as there are no switching events that would typically require smaller time steps and/or interpolation (or iterations) for accurately locating the opening or closing of the diodes in the circuit.

II. Detailed Analysis

Commonly used high-pulse-count converters include 6-, 12-, 18-, and 24-pulse configurations. To facilitate the discussion in this paper, it is convenient to start the detailed analysis of multi-pulse converters with a brief review on the well-established behavior of the 3-phase (6-pulse) bridge rectifier shown in Fig. 1. The system is composed of a balanced 3-phase source $\mathbf{e}_{abcs}$, commutating inductance L_c, six diodes $S_1 - S_6$, a dc-link filter r_{dc}, L_{dc}, C, and a load R_L. The voltage across the load is defined as e_d. Assuming balanced operation, the input phase voltages are

$$e_{as} = \sqrt{2}E\cos(\theta_e), \tag{1}$$

$$e_{bs} = \sqrt{2}E\cos\left(\theta_e - \frac{2\pi}{3}\right), \tag{2}$$

$$e_{cs} = \sqrt{2}E\cos\left(\theta_e + \frac{2\pi}{3}\right), \tag{3}$$

where θ_e is the electrical angle of the source, and E is the rms value of the phase voltage.

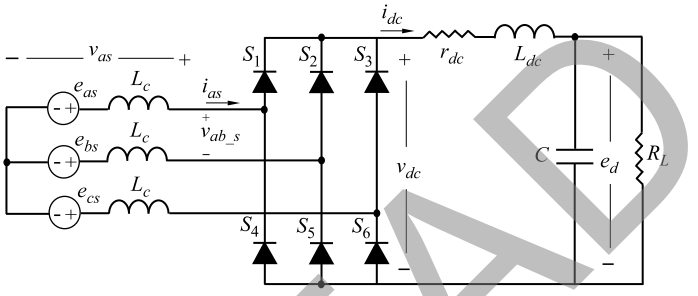

Fig. 1. Conventional 3-phase 6-pulse rectifier system.

As the load on the dc bus may change in a wide range, from a light load to a short circuit, three different switching patterns are observed for this system resulting in three operational modes [12]. The typical waveforms of the phase currents, corresponding to the three operational modes, are shown in Fig. 2. The corresponding waveforms of the dc bus voltage v_{dc} are sketched in Fig. 3.

As shown in Figs. 2 and 3, there exist six equal switching intervals within a single electrical cycle defined by θ_e. Within Mode 1, each switching interval is divided into two subintervals referred to as commutation and conduction [5]. During the conduction subinterval (t_{cond}) only two diodes conduct. During the commutation subinterval (t_{com}) corresponding to the commutation angle $\mu = t_{com} \cdot \omega_e$, three diodes conduct and the current is switched from one phase to another. Therefore, in Mode 1, a conduction pattern of 2-3 diodes is observed within each 60 electrical degrees, and $0^\circ < \mu < 60^\circ$. Mode 2 may be achieved by increasing the load current. In this mode, the commutation angle μ increases and reaches 60 degrees. This result in disappearance of the conduction subinterval and three diodes carry current throughout the switching intervals. This mode can be clearly observed in Fig. 3 (middle plot), wherein all intervals became uniform. If the load current is further increased, after a certain point the commutation angle μ starts to increase as well, and results in Mode 3. This changes the sequence of topologies and the switching pattern contains 3-4 conducting diodes. Note that this mode contains a topology with 4 simultaneously conducting diodes which momentary short-circuits the output dc voltage v_{dc} as depicted in Fig. 3 (bottom plot).

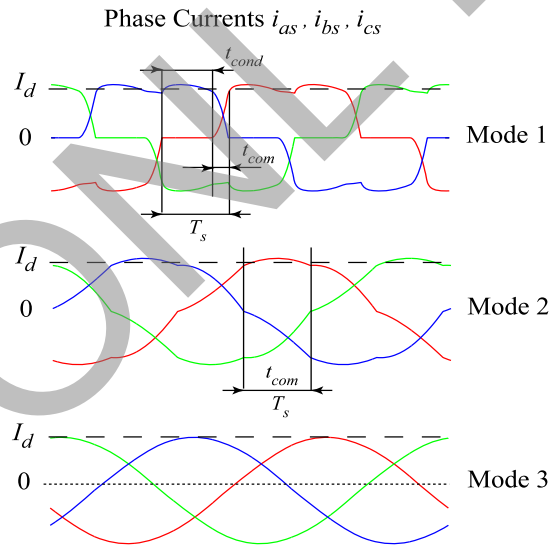

Fig. 2. Typical waveforms of phase currents in different operating modes.

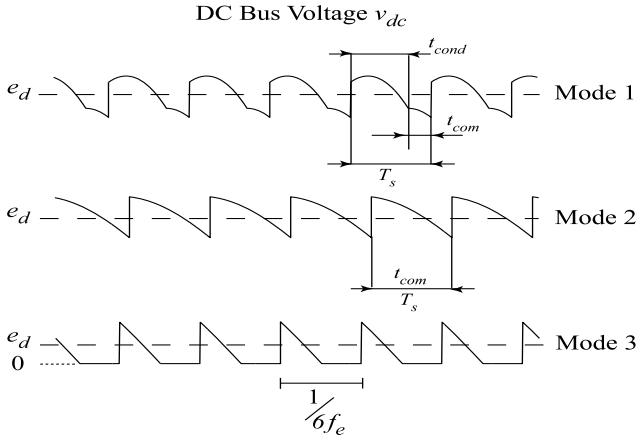

Fig. 3. Typical waveforms of dc bus voltage in different operating modes.

The operational modes depicted in Figs. 2 and 3 are summarized in Table I together with the corresponding commutation angle and the conduction pattern. To span these modes, one can vary the load from open circuit to short circuit, which is also depicted in the regulation characteristic in Fig. 4. Here, the dc output voltage V_d along the vertical

axis is scaled by the open-circuit voltage $V_{d0,3}$ and the dc output current I_d along the horizontal axis is scaled by the short-circuit current $I_{dsc,3}$. These quantities are calculated respectively as

$$V_{d0,3} = \frac{3\sqrt{6}E}{\pi}, \tag{4}$$

$$I_{dsc,3} = \frac{\sqrt{2}E}{\omega_e L_c}, \tag{5}$$

where ω_e is the electrical angular velocity of the source.

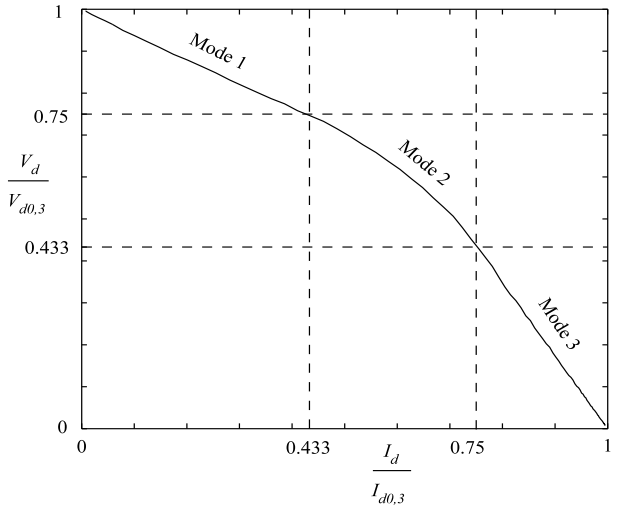

Fig. 4. Steady state regulation characteristic for the 3-phase 6-pulse bridge converter.

TABLE I
OPERATIONAL MODES OF THE CONVENTIONAL 3-PHASE 6-PULSE RECTIFIER

Operational Modes	Conduction Pattern	Commutation Angle
1	2-3	$0^\circ < \mu < 60^\circ$
2	3	$\mu = 60^\circ$
3	3-4	$60^\circ < \mu < 120^\circ$

Converters with higher pulse-count include 12-, 18-, and 24-pulse configurations, which are generally considered to improve the quality of dc voltage and current at the output terminals. For the purpose of this paper, a 6-phase 12-pulse rectifier shown in Fig. 5 is considered. A similar configuration may be achieved by utilizing two sets of wye/delta windings of a conventional 3-phase system (transformer and/or synchronous generator). Without the loss of generality, the two six-pulse bridges form a parallel connection. The displacement angle between the two 3-phase sets is commonly chosen to be 30 electrical degrees, however in certain applications the displacement angle may be 60 electrical degrees [13]. The configuration of the 12-pulse rectifier may also be varied by either including or excluding the Inter-Phase Transformer (IPT) and by connecting/disconnecting the neutral points of the two sets of 3-phase voltage sources. These configurations result in a more complicated switching pattern and a large number of operational modes which are more difficult to establish analytically [13], [14].

Modes of operation for the case of 30-degree displacement angle, disconnected neutrals, and without the inter-phase transformer, have been analytically established in [10] wherein a simplified case of constant dc bus current is assumed. These modes are summarized in Table II and the regulation characteristic for this case is shown in Fig. 6. Reference [10] also assumes a case with an ideal inter-phase transformer, i.e., the magnetizing reactance of the IPT is assumed to be infinite. Thus the load current will be equally shared between the two bridges which operate independently. Under these assumptions, the operational modes may be derived by analyzing one of the bridges with one-half of the load current [10]. Three modes of operation are then recognized which are summarized in Table III. It should be noted that in a case of non-ideal inter-phase transformer, the regulation characteristic will lie between these two extreme cases [10].

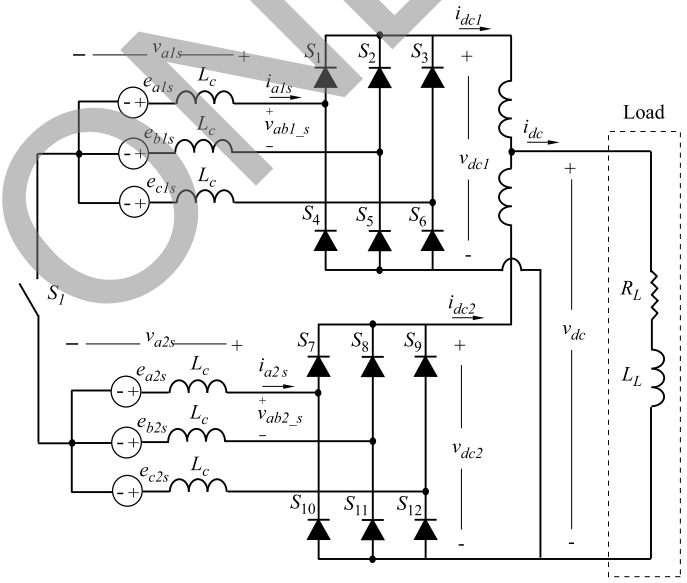

Fig. 5. Typical 6-phase 12-pulse bridge rectifier system.

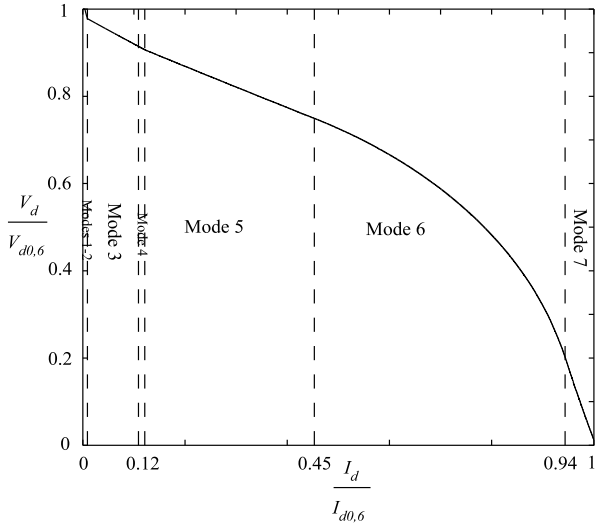

Fig. 6. Steady state regulation characteristic for the 6-phase 12-pulse bridge converter with the neutral points disconnected.

TABLE II
OPERATIONAL MODES OF THE 12-PULSE RECTIFIER

Operational Modes	Conduction Pattern
1	4-2
2	5-4-2-4
3	5-4
4	6-5-4-5
5	6-5
6	6
7	7-6

TABLE III
OPERATIONAL MODES OF THE 12-PULSE RECTIFIER WITH IDEAL IPT

Operational Modes	Conduction Pattern
1	4-2
2	5-4-2-4
3	5-4

If the neutral points of the two sets of 3-phase voltage sources in Fig. 5 are connected, a new set of line-to-line voltages is established between the phases. This will allow the phase current waveforms to become asymmetric resulting in more complicated operational modes. The regulation characteristic for this case is shown in Fig. 7 with the modes of operation summarized in Table IV.

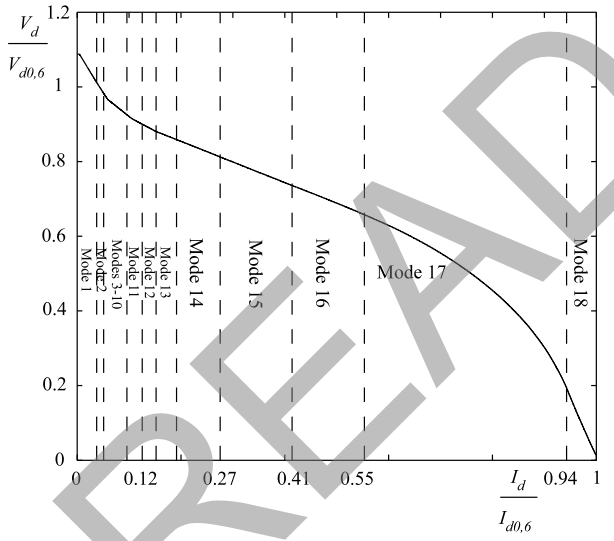

Fig. 7. Steady state regulation characteristic for the 6-phase 12-pulse bridge converter with connected neutral points.

TABLE IV
OPERATIONAL MODES OF THE 12-PULSE RECTIFIER WITH CONNECTED NEUTRAL POINTS

Operational Modes	Conduction Pattern
1	3-4-3-2
2	5-4-3-2-3-4
3	5-4-3-3-2-3-4
4	5-4-3-4-3-3-2-3-4
5	5-4-3-4-3-3-4
6	5-4-3-4-3-4-3-4
7	5-4-3-4-4-3-4
8	5-4-3-4-4
9	5-4-5-4-3-4
10	5-4-5-4-4
11	5-4
12	6-5-4-5-4-5
13	6-5-4-5
14	6-5-5
15	6-5-6-5
16	6-6-5
17	6
18	7-6

III. DYNAMIC AVERAGE-VALUE MODELING

To demonstrate the concept of dynamic average-value models, both 6- and 12-pulse converters are considered in this Section. Although analytically derived models and parametric models have their own benefits, disadvantages and challenges, both methodologies (if applied correctly) should lead to very similar results in predicting the averaged dynamic behavior of the detailed switching converter circuit. The two methodologies are briefly discussed and compared in this section.

A. Analytical Derivation

Deriving the AVM for line-commutated converters requires averaging of state variables over a switching interval. This in turn requires knowledge of the operating mode and its boundary conditions for which the respective averages will be valid. Therefore, there will be an AVM for each operating mode that is in the range of interest. Such models can then be "switched" as the system changes the modes, which makes this approach additionally challenging.

In most literature sources, the AVM is typically derived for one operating mode only [5], [6], [11]. For the 3-phase 6-pulse configuration of Fig. 1 the AVM is typically considered for Mode 1. The approach makes use of the so-called *qd* converter reference frame which facilitates the analysis. In this synchronous reference frame depicted in Fig. 8, the *d*-axis component of voltage is zero.

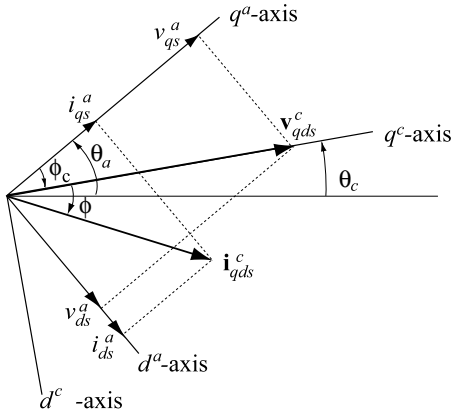

Fig. 8. Relationship among the variables in the converter and the arbitrary reference frames.

As shown in Fig. 8, the relationship between the voltages in the converter and the arbitrary reference frames may be written as

$$\begin{bmatrix} v_{qs}^{c} \\ 0 \end{bmatrix} = \begin{bmatrix} \cos(\phi_c) & \sin(\phi_c) \\ -\sin(\phi_c) & \cos(\phi_c) \end{bmatrix} \begin{bmatrix} v_{qs}^{a} \\ v_{ds}^{a} \end{bmatrix}. \tag{6}$$

The angle between the respective components of the voltage in the converter and the arbitrary reference frame may be deduced from Fig. 8 as

$$\phi_c = \tan^{-1}\left(\frac{v_{ds}^{a}}{v_{qs}^{a}}\right). \tag{7}$$

The next step is to derive the equations describing the dynamics of the dc bus. The dc bus voltage equation is expressed and averaged during the switching interval. Considering the KVL on the dc side, the state equation for the dc bus current is then obtained as

$$\frac{d\bar{i}_{dc}}{dt} = \frac{\frac{3\sqrt{3}}{\pi}\sqrt{2}E - \left(r_{dc} + \frac{3}{\pi}L_c\omega_e\right)\bar{i}_{dc} - e_d}{L_{dc} + 2L_c}. \tag{8}$$

To establish the average *q*- and *d*-axes components of the phase currents on the ac side, the dc current is typically assumed constant throughout the switching interval. The currents are then expressed during each subinterval (i.e., conduction and commutation) and averaged over the respective subintervals. The commutation and conduction components of the averaged ac currents are then obtained. The result of this procedure yields the following equations [5]:

$$\bar{i}_{qs,com}^{c} = \frac{2\sqrt{3}}{\pi}\bar{i}_{dc}\left[\sin\left(\mu - \frac{5\pi}{6}\right) + \sin\left(\frac{5\pi}{6}\right)\right] + \frac{3}{\pi}\frac{\sqrt{2}E}{L_c\omega_e}(\cos\mu - 1) + \frac{3}{4\pi}\frac{\sqrt{2}E}{L_c\omega_e}(1 - \cos(2\mu)), \tag{9}$$

$$\bar{i}_{ds,com}^{c} = \frac{2\sqrt{3}}{\pi}\bar{i}_{dc}\left[-\cos\left(\mu - \frac{5\pi}{6}\right) + \cos\left(\frac{5\pi}{6}\right)\right] + \frac{3}{\pi}\frac{\sqrt{2}E}{L_c\omega_e}\sin\mu - \frac{3}{4\pi}\frac{\sqrt{2}E}{L_c\omega_e}(\sin(2\mu) + 2\mu), \tag{10}$$

$$\bar{i}_{qs,cond}^{c} = \frac{2\sqrt{3}}{\pi}\bar{i}_{dc}\left[\sin\left(\frac{7\pi}{6}\right) - \sin\left(\mu + \frac{5\pi}{6}\right)\right], \tag{11}$$

$$\bar{i}_{ds,cond}^{c} = \frac{2\sqrt{3}}{\pi}\bar{i}_{dc}\left[-\cos\left(\frac{7\pi}{6}\right) + \cos\left(\mu + \frac{5\pi}{6}\right)\right]. \tag{12}$$

The final currents are obtained by adding the contributions from both commutation and conduction subintervals as

$$\bar{i}_{qs}^{c} = \bar{i}_{qs,com}^{c} + \bar{i}_{qs,cond}^{c}, \tag{13}$$

$$\bar{i}_{ds}^{c} = \bar{i}_{ds,com}^{c} + \bar{i}_{ds,cond}^{c}. \tag{14}$$

A similar model has been derived in [11] where the dynamics are reported to be improved. There, instead of assuming a constant value for the dc current throughout the switching interval, it has been assumed that the current changes linearly. In particular, using the first order Taylor series expansion, the dc current is written as [11]

$$i_{dc}(\theta) = i_{dc0} + k\cdot\left(\theta - \frac{\mu}{2}\right), \tag{15}$$

where i_{dc0} is the average value of i_{dc} during the commutation period and k is the derivative of $di_{dc}/d\omega_e t$ during this period of time. The remaining steps taken to derive the AVM are similar to those discussed above, and the resulting model is expressed as follows:

$$\frac{d\bar{i}_{dc}}{dt} = \frac{\frac{3\sqrt{3}}{\pi}\sqrt{2}E - \left(r_{dc} + \frac{3}{\pi}L_c\omega_e\right)i_{dc0} - e_d}{L_{dc} + L_c\left(2 - \frac{3\mu}{2\pi}\right) + \frac{r_{dc}}{2\omega}\left(\frac{\pi}{3} - \mu\right)}, \tag{16}$$

$$\bar{i}_{qs}^{c} = \frac{2\sqrt{3}}{\pi}i_{dc0}\cos\mu + \frac{\sqrt{3}}{\pi}k\left(\sin\mu - \frac{\pi}{3}\right) - \frac{3}{\pi}\frac{\sqrt{2}E}{\omega_e L_c}\left(\cos\mu - \frac{\cos(2\mu)}{4} - \frac{3}{4}\right), \tag{17}$$

$$\bar{i}_{ds}^{c} = \frac{2\sqrt{3}}{\pi}i_{dc0}\sin\mu - \frac{\sqrt{3}}{\pi}k\left(1 + \cos\mu - \frac{\sqrt{3}\pi}{3}\right) + \frac{3}{\pi}\frac{\sqrt{2}E}{\omega_e L_c}\left(-\sin\mu + \frac{\mu}{2} + \frac{\sin(2\mu)}{4}\right). \tag{18}$$

Finally, the first model is defined by (8)–(14) and is referred to as AVM#1, and the second model is defined by (16)–(18) and is referred to as AVM#2. Both analytically-derived AVMs utilize the same commutation angle given by:

$$\mu = \cos^{-1}\left(1 - \frac{\sqrt{2}L_c\omega_e}{\sqrt{3}E}i_{dc0}\right). \tag{19}$$

Although an improvement has been reported in the dynamics of the AVM#2, the new model is still valid for Mode 1 only as it has been obtained considering two subintervals.

B. Parametric Method

Herein, instead of deriving analytical equations for the system, the AVM parametric functions are obtained numerically based on detailed time-domain simulation. Similar to the previous method, the three phase voltages are taken to the converter reference frame, using appropriate transformation (6). Since the rectifier switching cell does not contain energy-storing elements, its average-value model may be considered as an algebraic block which relates the averaged dc-link variables on one side and the averaged ac variables transferred to the converter reference frame at the other side. The averaged rectifier dc voltage $\bar{v}_{dc}$ and current $\bar{i}_{dc}$ are related to $\bar{\mathbf{v}}_{qds}^{c}$ and $\bar{\mathbf{i}}_{qds}^{c}$ through the respective parametric function as

$$\left\|\bar{\mathbf{v}}_{qds}^{c}\right\| = \alpha(\cdot)\,\bar{v}_{dc}, \tag{20}$$

$$\bar{i}_{dc} = \left\| \bar{\mathbf{i}}^{c}_{qds} \right\| \beta(\cdot), \tag{21}$$

where $\alpha(.)$ and $\beta(.)$ are algebraic functions of the loading conditions. Also from Fig. 8, the angle between the vectors $\bar{\mathbf{v}}^{c}_{qds}$ and $\bar{\mathbf{i}}^{c}_{qds}$ may be expressed as

$$\phi(\cdot) = \tan^{-1}\left(\frac{\bar{i}^{a}_{ds}}{\bar{i}^{a}_{qs}}\right) - \tan^{-1}\left(\frac{\bar{v}^{a}_{ds}}{\bar{v}^{a}_{qs}}\right). \tag{22}$$

Deriving closed-form analytical expressions for $\alpha(.)$, $\beta(.)$, and $\phi(.)$ is impractical. Instead, these functions may be extracted using the simulation results. It is convenient to express these functions in terms of dynamic impedance of the converter switching cell as

$$z = \frac{\bar{v}_{dc}}{\left\| \bar{\mathbf{i}}^{c}_{qds} \right\|}. \tag{23}$$

Using (20)–(22), functions $\alpha(.)$, $\beta(.)$, and $\phi(.)$ are extracted for a wide range of operating points. A transient study may be carried out in which the load resistance is slowly changed in a wide range. The numerical functions $\alpha(z)$, $\beta(z)$, and $\phi(z)$ together with the impedance z, are then calculated for each point using (20)–(23). These functions are stored in a look-up table and used in the average-value model implementation.

IV. Computer Studies

In order to investigate the behavior of the AVMs discussed in the previous Section, these models together with the detailed switch-level models have been implemented in the MATLAB/Simulink and the PSCAD/EMTDC as these simulation packages are commonly considered for detailed modeling of power systems with power electronic converters [15]. The results obtained by both simulation packages were virtually identical with some adjustments in time step to achieve similar accuracy. As an example, Fig. 9 shows the parametric average-value model implemented in the PSCAD/EMTDC environment. As seen in this figure, the voltage source is modeled in the converter reference frame (top block) with the *qd* currents as outputs and *qd* voltages as inputs. The inputs to the rectifier AVM are the *qd* currents, at the ac side, and the dc bus voltage, whereas the outputs are the *qd* voltages and the dc bus current.

A. Six-Pulse Converter

Here, the 3-phase rectifier system is assumed to operate initially in a steady state condition with a $10\,\Omega$ load resistor. Then, at $t = 0.5\,s$, the load resistance is stepped to $1\,\Omega$. The corresponding transient responses predicted by detailed and average-value models are shown in Fig. 10. During the transient, the converter operation remains within Mode 1. As can be seen in Fig. 10, since the operational mode is not changed, the average-value models can predict the response of the system with reasonable accuracy, i.e., the AVMs responses go through the ripple of the waveforms predicted the detailed model.

Next, the load resistance is stepped from $1\,\Omega$ to $0.1\,\Omega$, which results in a change of the operational mode from Mode 1 to Mode 2. The corresponding transient responses predicted by detailed and average-value models are shown in Fig. 11. As expected, the responses predicted by the analytically-derived AVMs all fail to correctly predict the transition to Mode 2 as these models have been derived with the assumption of conduction-commutation pattern of Mode 1. However, the parametric AVM remains valid and predicts the response close to that of the detailed switching model.

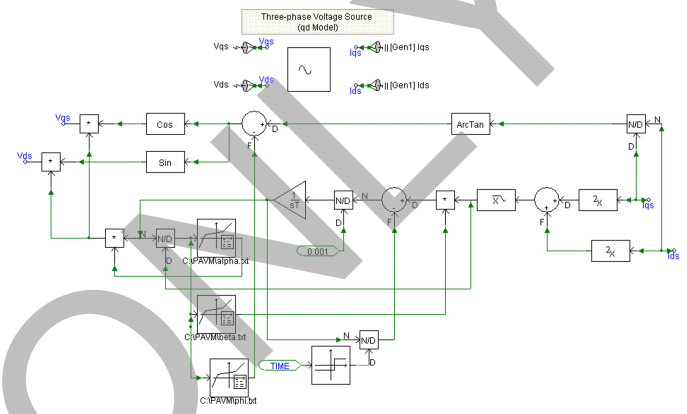

Fig. 9. Parametric average-value model implemented in the PSCAD/EMTDC.

B. Twelve-Pulse Converter

Simulation studies of the twelve-pulse rectifier have been conducted using the detailed model and the parametric AVM only since the analytically-derived models do not capture the inter-mode transitions. A similar study has been carried out in which the load resistance is stepped from $1\,\Omega$ to $0.1\,\Omega$ at $t = 0.5\,s$. The corresponding responses, for the case of connected neutral points, are superimposed in Fig. 12. In this case, the operational mode is changing from Mode 13 (i.e., 6-5-4-5 conduction pattern) to Mode 17 (6-valve conduction pattern), and as Fig. 12 shows the AVM predicts the transient response very accurately.

V. Summary and Conclusions

To evaluate the effectiveness of the AVMs relative to the switching models, one can compare the time-step size and the total number of time steps that were required by each of the models to complete the entire transient response. For the purpose of comparison in this Section, transient study duration of 1 sec was assumed. For example, in case of 6-pulse rectifier the time steps taken by each of the models implemented in Simulink are summarized in Table V. All Simulink models were executed using variable time-step solver that can automatically adjust the step size during the transient. As can be seen in Table V, the switching model required the largest number of time steps (22,659), which was

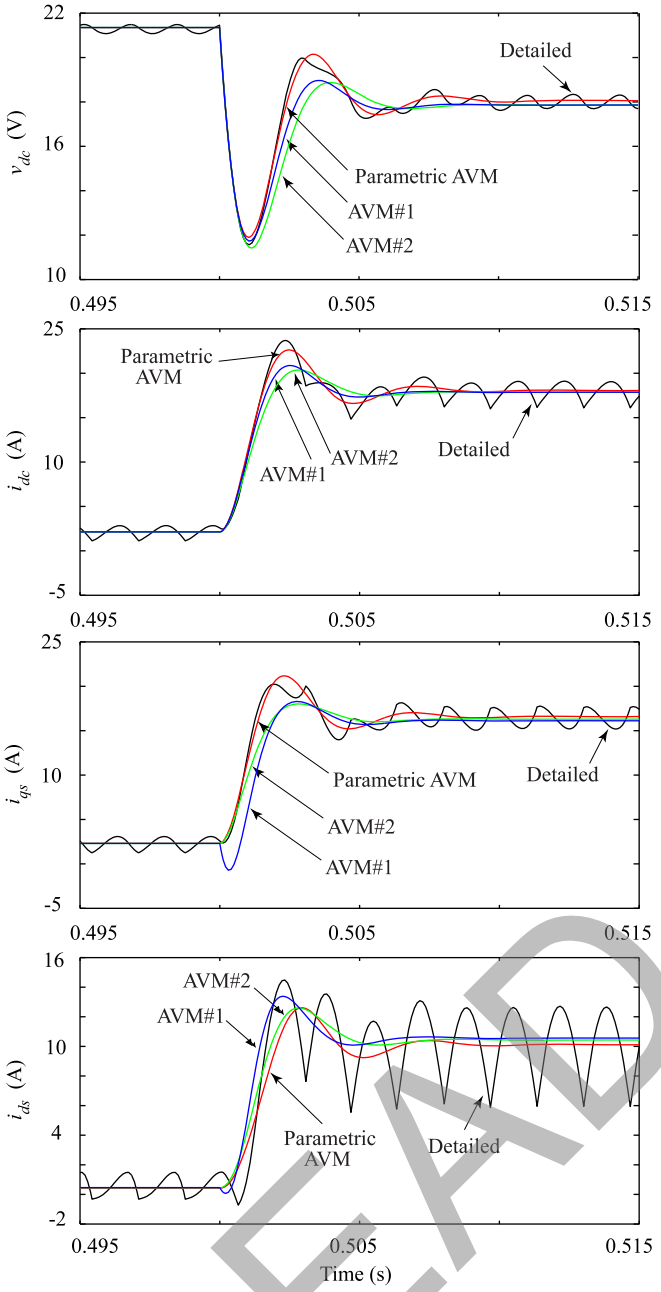

Fig. 10. Six-pulse converter transient response within Mode 1 as predicted by detailed and averaged models.

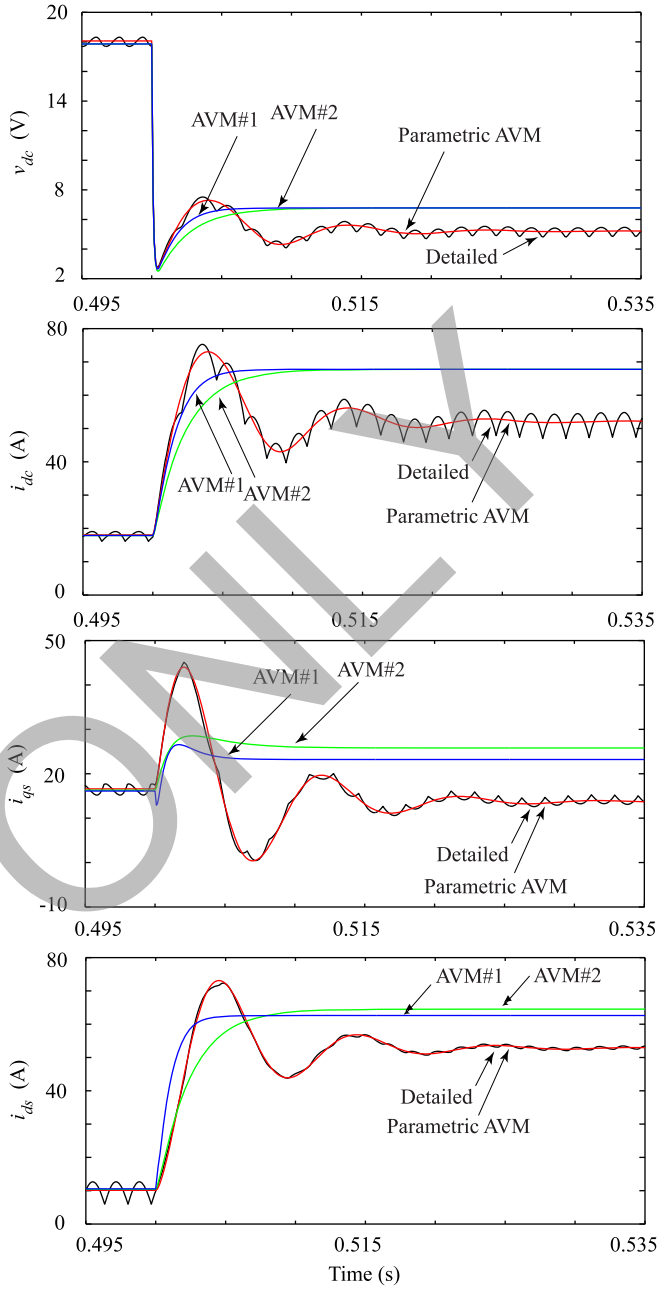

Fig. 11. Six-pulse converter transient response from Mode 1 to Mode 2 as predicted by detailed and averaged models.

needed in order to accurately handle all the switching events (discontinuities). The AVMs could utilize a much larger time step since these models are continuous, taking much fewer steps (281, 271, and 309, respectively).

The studies with 12-pulse rectifier were carried out using both PSCAD and Simulink. The summary of the time steps is given in Table VI. For the considered time interval/study of 1 sec, the detailed model again took the largest number of steps (20,001 and 15,366). There is some difference between the PSCAD and Simulink detailed models, which is attributed to the fact that PSCAD uses fixed time-step to solve the entire transient, whereas Simulink can vary the time-step to accommodate the switching and other transients.

The detailed-PSCAD model was run with a typical EMTP time-step of 50 micro-second required to properly handle the switching of diodes. However, the AVM-PSCAD and AVM-Simulink could use appreciable larger time steps, which altogether demonstrates the benefits of the AVM approach where each model took significantly fewer time steps (5586 and 194). The AVM-PSCAD could not run at very large time steps because the time-step was still limited by the relatively fast transient observed during the rapid change in the load.

As shown in this paper, such dynamic average models can be very effective for simulations of systems transients where the switching harmonics injected into the ac grid or the dc link are neglected. Including the effect of switching harmonics would require a special consideration and may be pursued in

combination with other approaches e.g. multiple reference frames, harmonic-domain modeling, etc.

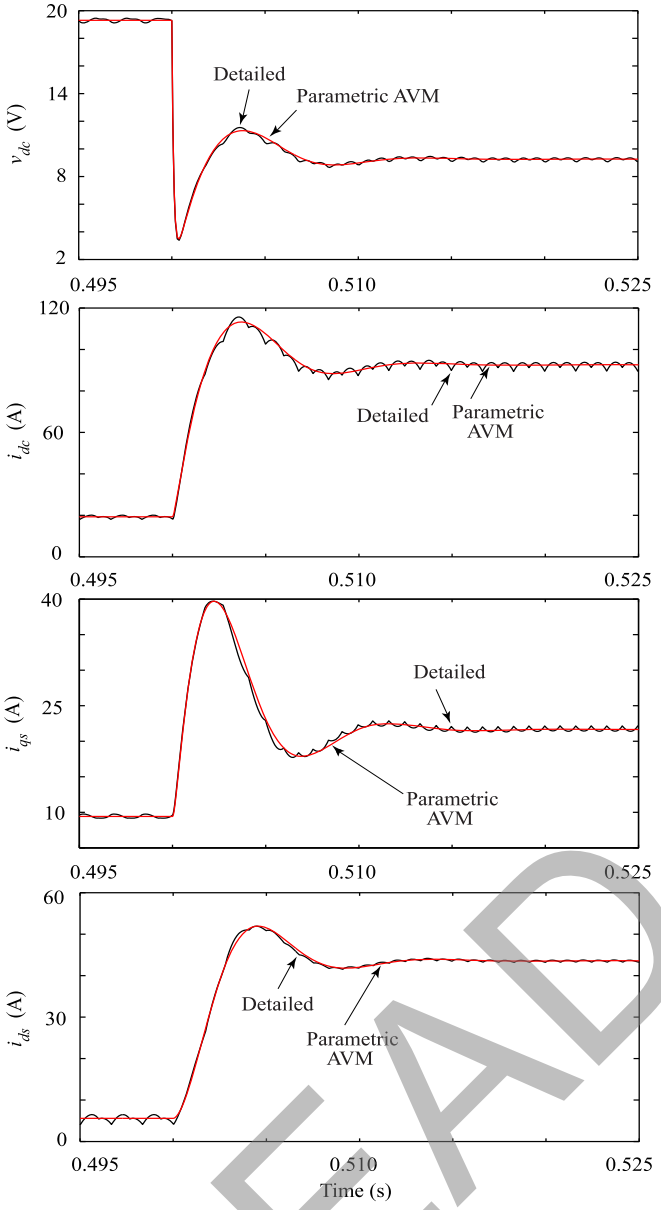

Fig. 12. Twelve-pulse converter transient response from mode 13 to mode 17 as predicted by detailed and averaged models.

TABLE V
COMPARISON OF SIMULATIONS FOR THE 6-PULSE RECTIFIER

Model	Time Steps
Detailed Model	22,659
AVM #1	281
AVM #2	271
Parametric AVM	309

TABLE VI
COMPARISON OF SIMULATIONS FOR THE 12-PULSE RECTIFIER

Model	Time Steps
Detailed - PSCAD	20,001
Detailed - Simulink	15,366
AVM - PSCAD	5586
AVM - Simulink	194

VI. APPENDIX

Parameters for the rectifier circuits used in this paper:

$$\sqrt{2}E = 13.2\ V\ ,\ \omega_e = 2\pi 100\ ,\ L_c = 0.37\ \text{mH}\ ,\ C = 1\ \text{mF}\ .$$

VII. REFERENCES

[1] *PSCAD/EMTDC V4.0 On-Line Help,* Manitoba HVDC Research Centre and RTDS Technologies Inc., 2005.

[2] "SimPowerSystems: Model and simulate electrical power systems," User's Guide, The MathWorks Inc., 2006 (www.mathworks.com).

[3] "Piecewise Linear Electrical Circuit Simulation (PLECS)," User Manual Ver. 1.4, Plexim GmbH (www.plexim.com).

[4] "Automated State Model Generator (ASMG)," Reference Manual Version 2, P C Krause & Associates, Inc. 2003 (www.pcka.com).

[5] P. C. Krause, O. Wasynczuk, and S. D. Sudhoff, *Analysis of Electric Machinery and Drive Systems*, Piscataway, NJ: IEEE Press, 2002.

[6] S. D. Sudhoff, K. A. Corzine, H. J. Hegner, and D. E. Delisle, "Transient and dynamic average-value modeling of synchronous machine fed load-commutated converters," IEEE Trans. Energy Conv., vol. 11, pp. 508–514, Sept. 1996.

[7] I. Jadric, D. Borojevic, and M. Jadric, "Modeling and control of a synchronous generator with an active DC load," IEEE Trans. Power Electron., vol. 15, pp. 303–311, March 2000.

[8] J. Jatskevich, S. D. Pekarek, and A. Davoudi, "Parametric average-value model of synchronous machine-rectifier systems," *IEEE Trans. Energy Conversion,* vol. 21, no. 1, Mar. 2006.

[9] B. Zhang, and S. D. Pekarek, " Analysis and average value model of a source-commutated 5-phase rectifier", IEEE PESC 2004, Aachen Germany, 2004.

[10] Y. Tzeng, N. Chen, and R. Wu, "Modes of operation in parallel-connected 12-pulse uncontrolled bridge rectifiers without an interphase transformer", *IEEE Trans. Industrial Electronics,* vol. 44, no. 3, Jun. 1997.

[11] H. Zhu, R. P. Burgos, F. Lacaux, A.Uan-Zo-li, D.K. Lindner, F. Wang, and D. Boroyevich, "Average modeling of three-phase and nine-phase diode rectifiers with improved ac current and dc voltage dynamics", IECON 2005, Nov. 2005.

[12] R. M. Davis, *Power Diode and Thyristor Circuits*, Cambridge at the University Press, 1971.

[13] J. Jatskevich, and S. D. Pekarek, " Six-phase synchronous generator-rectifier parametric average value modeling considering operational modes", *HAIT Journal of Science and Engineering B*, vol. 2, no. 3-4, pp. 365-385, 2005.

[14] J. Jatskevich, O. Wasynczuk, E. A. Walters, C. E. Lucas, S. D. Pekarek, and P. T. Lamm, "Automated identification of the operational modes of switched electric circuits", *SAE Transactions, Journal of Aerospace,* Sect. 1, Set 3, pp. 955–961, 2000.

[15] M. O. Faruque, Y. Zhang, V. Dinavahi, "Detailed modeling of CIGRE HVDC benchmark system using PSCAD/EMTDC and PSB/SIMULINK", *IEEE Trans. on Power Delivery*, vol. 21, no. 1, pp. 378–387, Jan. 2006.